SIZE DEPENDENT EFFECTS

Electrocatalytic behavior of Ni-based amorphous alloys for hydrogen evolution

L. Mihailov · T. Spassov · I. Kanazirski · I. Tsvetanov

Abstract Ni-based amorphous alloys were synthesized by rapid quenching from the melt, using a planar flow technique. Their amorphous nature and thermal stability were studied by X-ray diffraction and differential scanning calorimetry. The electrocatalytic activity of the as-quenched amorphous alloys with respect to the hydrogen evolution reaction (HER) in alkaline water electrolysis was studied in relation to the alloy composition. The kinetic parameters of the HER were evaluated by cyclic voltammetry and impedance spectroscopy techniques in 6 M KOH at room temperature. The electrocatalytic activity of the amorphous alloys was found to depend on the alloy composition. It was obtained that molybdenum containing amorphous alloys (Ni–Mo–B) showed a superior electrocatalytic activity in the HER compared to Ni–(Nb,Ta)–B and Ni–Si–B, as $Ni_{66.5}Mo_{28.5}B_5$ revealed considerably lower charge transfer resistance and higher exchange current density than $Ni_{63}Mo_{27}B_{10}$. The results have to be attributed to an improved intrinsic activity of the Ni–Mo–B alloys compared to the other Ni-based glasses.

Introduction

It is known that amorphous metallic alloys exhibit promising electrocatalytic properties for hydrogen evolution, as well as for oxygen evolution in alkaline water solutions [1–8]. The interest to these thermodynamically unstable materials comes from the possibility to prepare alloys with different composition, e.g., containing various attractive from electrocatalytic point of view elements. Furthermore, the amorphous alloys usually reveal improved corrosion resistance compared to their crystalline counterparts, due to the lack of phase and grain boundaries and other typical for the crystalline materials defects. Their good mechanical properties are also among the reasons to select amorphous alloys for electrochemical applications [8]. Ni-based amorphous alloys are among the most studied materials for hydrogen evolution [1, 5–7].

Shan et al. [1] reported that owing to the larger exchange current densities and larger surface roughness, the amorphous Ni–S–Mn alloy electrode performs at a higher electrochemical activity with greater stability for the hydrogen evolution reaction (HER) in 30 wt% KOH solution than the Ni–S alloy electrode. To enhance the electrocatalytic activity of the amorphous alloys, they are often chemically treated in different solutions. Gebert et al. [5] studied rapidly solidified Ni–Nb–Y amorphous alloys for HER. They reported that the main effect of a HNO_3/HF solution treatment is a selective dissolution of Y-rich phases, leading to an excavation of the lower reactive Nb-rich phase regions. The authors also found that in strongly alkaline environment the as-quenched two-phase amorphous ribbon surfaces are quite inactive and blocked by a strong passive layer. The enhanced reactivity of etched Ni–Nb–Y ribbons can be mainly related with the high reactivity of the residual Y-rich matrix phase [5]. The electrocatalytic behavior of $Zr_{100-y}Ni_y$ alloys with $y = 33$ and $y = 60$ for the HER was studied in relation to both the composition and the active surface area of the electrodes in the as-quenched state and after treatment with HF [6]. The high electrode activity after chemical treatment was related

L. Mihailov · T. Spassov (✉) · I. Tsvetanov
Faculty of Chemistry, University of Sofia "St. Kl. Ohridski",
1 James Bourchier str., 1164 Sofia, Bulgaria
e-mail: tspassov@chem.uni-sofia.bg

I. Kanazirski
University of Mining and Geology "St. Ivan Rilski", 1172 Sofia, Bulgaria

to the increase in the intrinsic activity of the porous electrode surface of a Raney-type structure, formed on the Zr–Ni alloy surface. Kirk et al. [7] have studied the role of the structure and chemistry of Ni-based amorphous alloys on the electrochemical activity for HER in alkaline electrolysis. They found that the best parameter to correlate with the electrocatalytic activity was the short range order value of the amorphous alloys.

Electrodeposited Ni-based composite coatings are also usually characterized by high electrocatalytic activity for HER and good corrosion resistance in aggressive environments [9–14]. It is shown that deposited Ni + Mo composite coatings exhibit more porous surface morphology and higher activity towards the HER than pure Ni deposits [12]. The main contribution to the apparent activity is found to come from the surface area increase, although some improvement in the intrinsic activity is also observed [12]. Realizing the main contribution of the real surface area to the total electrochemical activity, different leachable elements (Al, Zn, Ti, etc.) were used successfully to produce Ni-Raney alloys electrodes for HER [15–18].

Metallurgically prepared multiphase Ni–Mo alloys were also found to be attractive for the HER [19], as among the investigated Ni–Mo alloys, such as MoNi, $MoNi_2$, $MoNi_3$, and $MoNi_4$ intermetallic compounds only MoNi exhibits considerably higher catalytic activity than Mo and Ni electrodes for HER in 1.0 mol dm^{-3} NaOH solution. Rate determining step of Heyrovsky was obtained at all investigated Ni–Mo electrodes. A strong influence of the microstructure on the electrocatalytic activity was reported for Ni–RE (RE = Ce, Pr, Y) crystalline alloys [20]. The presence of Ni primary crystals enhances the hydrogen adsorption at the electrode surface, leading to an increase of the hydrogen evolution kinetics. Interesting electrocatalytic properties are obtained with $Ni_{94}Pr_6$ and $Ni_{95}Ce_5$ electrodes, which exhibit the highest activities towards the HER. This behavior may be ascribed to a pronounced synergetic effect between nickel and Ni_5RE intermetallic compounds.

The present work aims at studying Ni-based rapidly solidified amorphous alloys as electrocatalysts for hydrogen evolution in alkaline water solution. Two groups of amorphous alloys have been investigated: the first one is based on the eutectic composition in the Ni–B system ($Ni_{81.5}B_{18.5}$) with Nb and Ta as alloying elements and the second comprises two Ni–Mo–B alloys with different Mo content ($Ni_{66.5}Mo_{28.5}B_5$ and $Ni_{63}Mo_{27}B_{10}$). Mo is known as an element, which improves the electrochemical behavior (corrosion resistance) of Ni-based alloys. Nb and Ta are less electronegative than Ni and although in small amounts may have a positive influence on the electrocatalytic activity of the Ni alloys. For comparison, Ni-based Ni–Si–B amorphous alloy was also studied for HER in the present work.

Experimental part

The alloys were prepared by melting of high purity Ni (99.99), Nb (99.9), Ta (99.9), B (99.9), and Si (99.999) in an induction furnace under pure argon atmosphere. From the master alloy ingots ribbons were produced by melt-spinning with an approximate quenching rate of 30 m/s. The chemical composition of the as-cast alloys was examined by SEM (JEOL-5510) with an energy dispersive X-ray analysis (EDX) and was found to correspond to the composition, assigned during the synthesis of the amorphous ribbons. The surface chemical information was obtained from X-ray photoelectron spectroscopy (XPS) using a VG ESCALAB II electron spectrometer under base pressure of 1×10^{-8} Pa. The photoelectron spectra were excited using un-monochromatized Al K_α radiation ($hv = 1486.6$ eV) with a total instrumental resolution of 1 eV. The C1s line of adventitious carbon at 285 eV was used as internal standard to calibrate the binding energies. The microstructure of the melt-spun materials in the as-quenched and annealed state was characterized by X-ray diffraction (XRD), using Bruker D8 Advance diffractometer with Cu K_α radiation. The thermal stability of the rapidly solidified alloys was studied by means of DSC (Perkin-Elmer DSC7) under pure argon atmosphere.

The HER on the amorphous ribbons was studied by means of steady-state polarization measurements and electrochemical impedance spectroscopy (EIS) using PARSTAT 2273 electrochemical (galavanostat/potentiostat) system. The electrolyte was 6 M KOH water solution. Three-electrode cell with Hg/HgO as a reference electrode and counter electrode prepared from Ni mesh was used for the electrochemical experiments. The amorphous ribbon electrode with 1 cm^2 surface area and thickness of 40 μm was mechanically polished by 1200 mesh abrasive paper. For each amorphous alloy, minimum two "current-overpotential" cycles were performed to ensure the reproducibility of the measurements.

The electrochemical impedance (IE) measurements were carried out in the frequency range of 100 kHz to 0.1 Hz and amplitude of the ac signal 10 mV. The impedance data were analyzed using ZSimpWin software. Electrochemical hydrogen charging and discharging were conducted at constant current density of 100 and 25 μA cm^{-2}, respectively. Cut off voltage was −400 mV.

Results and discussion

The nickel-based alloys in the present study, prepared by rapid solidification from a melt, reveal an amorphous structure. Figure 1 shows the X-ray diffraction patterns of the as-cast metallic ribbons. The amorphous nature of the
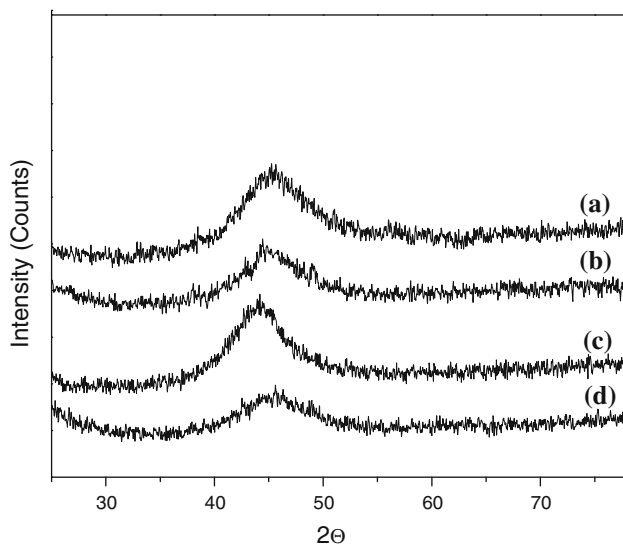
Fig. 1 X-ray diffraction pattern of as-quenched $Ni_{68}Si_{10}B_{22}$ (*a*), $Ni_{78.5}Ta_3B_{18.5}$ (*b*), $Ni_{63}Mo_{27}B_{10}$ (*c*) and $Ni_{78.5}Nb_3B_{18.5}$ (*d*)

as-prepared alloys as well as their thermal stability was also studied by DSC. The investigated glasses are characterized with relatively high crystallization temperatures (>400 °C).

Cyclic voltammograms at a potential sweep rate of 5 mV/min from a more positive potential of the working electrode compared to the hydrogen reversible potential (0.975 V vs. Hg/HgO) were carried out in order to obtain cathodic polarization curves of the HER for the amorphous alloys studied, Fig. 2. The dependence of the current density, *i*, on the overpotential, *η*, in Tafel coordinates is presented in Fig. 3 for all investigated alloys. A single cathodic Tafel slope, b_c, was observed for the Ni–Mo–B alloys (and partly for Ni–Si–B), whereas for the Ni–(Ta,Nb)–B alloys, there was a clear evidence for a large increase of b_c at about $\eta = -0.1$ V followed by a strong decrease at about $\eta = -0.25$ V. From the polarization curves of Fig. 3, the values of the exchange current density, i_o, and the Tafel slope, b_c, were determined and together with the hydrogen overpotential at $i = 10$ mA cm^{-2}, η_{10}, are presented in Table 1. The exchange current density i_o for $Ni_{66.5}Mo_{28.5}B_5$ has higher value compared to that of $Ni_{63}Mo_{27}B_{10}$, but is lower than i_o of pure crystalline Ni. The η_{10} for all investigated amorphous alloys are higher than that of crystalline Ni.

To investigate more carefully the interfacial properties of the amorphous Ni-based alloys, wide frequency range electrochemical impedance experiments were carried out. The results for all alloys studied are presented in Figs. 4 and 5 in Nyquist coordinates. Figure 4 shows the impedance spectra of the Ni–Mo–B alloy at different electrode overpotentials, and Fig. 5 presents the spectra for the different alloys at the same overpotential of −0.15 V, which
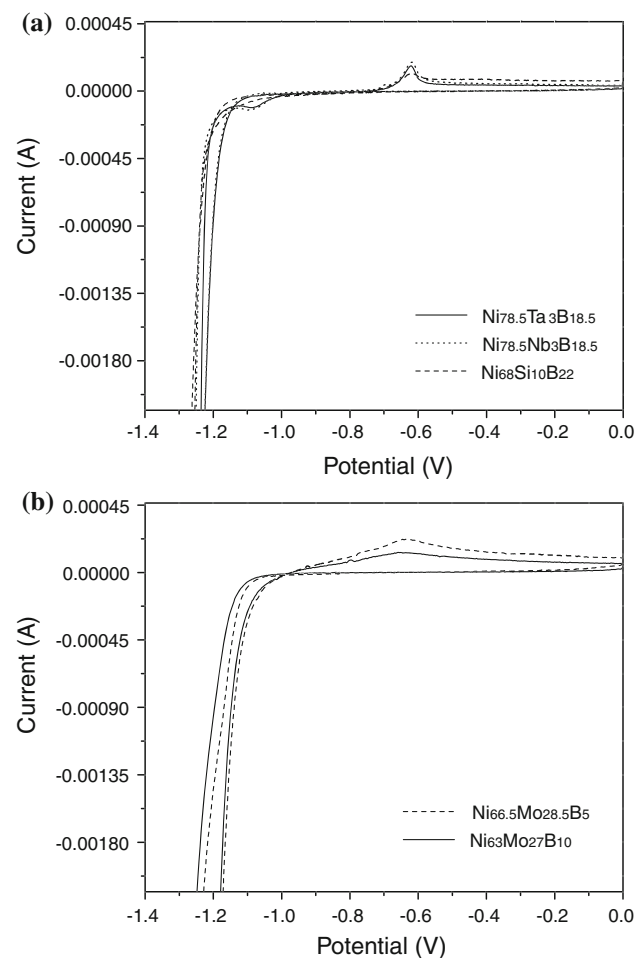

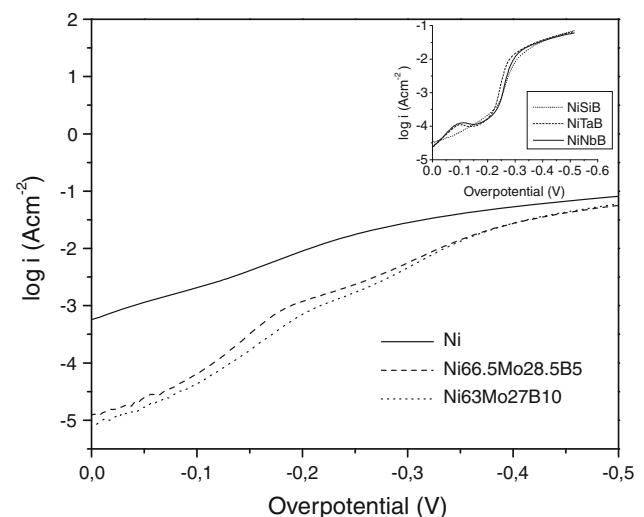Fig. 2 Voltammograms of the amorphous alloys studied in 6 M KOH at 25 °C

Fig. 3 Tafel plots for the as-quenched Ni-based amorphous alloys studied

Table 1 Kinetic parameters for the HER for Ni-based amorphous alloys in 6 M KOH at 25 °C

Working electrode	b_c (V dec^{-1})	I_0 (A cm^{-2})	η_{10} (mV)
Ni	−0.177	5.9×10^{-4}	190
Ni$_{66.5}$Mo$_{28.5}$B$_5$	−0.127	1.0×10^{-5}	247
Ni$_{63}$Mo$_{27}$B$_{10}$	−0.132	7.2×10^{-6}	250
Ni$_{78.5}$Ta$_3$B$_{18.5}$	–	–	267
Ni$_{78.5}$Nb$_3$B$_{18.5}$	–	–	279
Ni$_{68}$Si$_{10}$B$_{22}$	–	–	294

Table 2 Results for the R_{ct} (charge transfer resistance) and C_{dl} (double layer capacitance), obtained by fitting the experimental EIS data with the Randle model

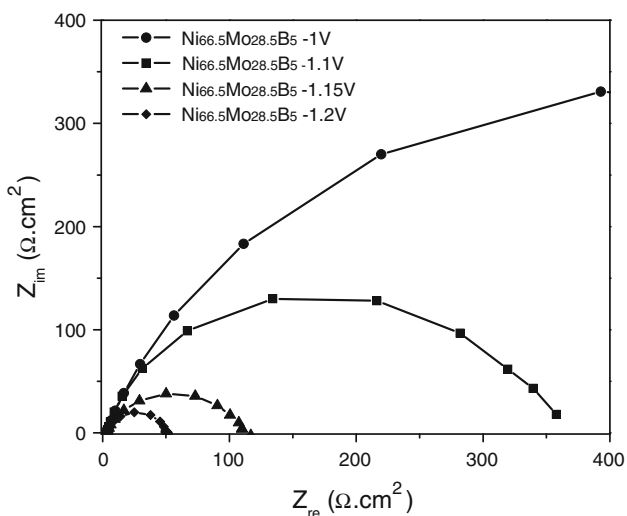| Working electrode	R_{ct} (Ω cm^2)	C_{dl} (μF cm^{-2})	η (V)
Ni$_{66.5}$Mo$_{28.5}$B$_5$	98	51.5	−0.15
Ni$_{63}$Mo$_{27}$B$_{10}$	446	46.0	−0.15
Ni$_{78.5}$Ta$_3$B$_{18.5}$	733	33.1	−0.15
Ni$_{78.5}$Nb$_3$B$_{18.5}$	1130	41.2	−0.15
Ni$_{68}$Si$_{10}$B$_{22}$	2596	32.0	−0.15

Fig. 4 Nyquist diagrams at different potentials for the Ni$_{66.5}$Mo$_{28.5}$B$_5$ amorphous alloy
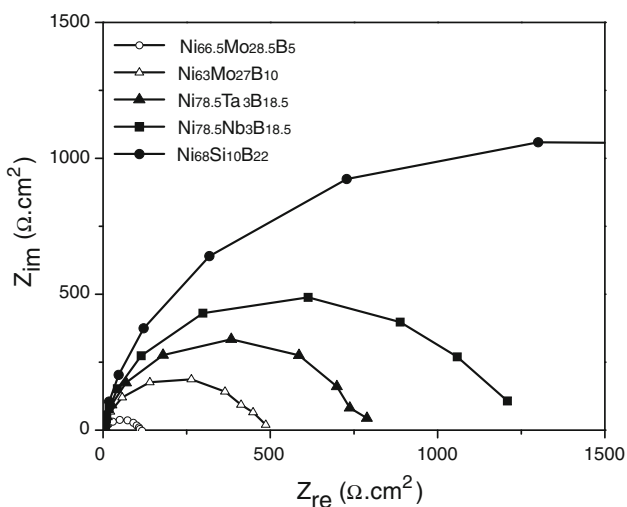

Fig. 5 Nyquist diagrams at $\eta = -0.15$ V for all investigated Ni-based amorphous alloys

is selected to be in the potential region of the Tafel reaction for Ni–Mo–B. All impedance curves can be satisfactorily described by a single time constant, indicating a kinetically controlled reaction. The electrical equivalent circuit used for simulating the experimental impedance spectra includes double layer capacitance (C_{dl}), charge transfer resistance (R_{ct}), and the electrolyte resistance (R_{el}), so-called Randles model. The values of the fitted parameters of the electrical equivalent circuit elements are presented in Table 2. As seen from Table 2, Ni$_{66.5}$Mo$_{28.5}$B$_5$ shows the lowest charge transfer resistance R_{ct} of about 100 Ω cm^2 and the amorphous Ni–Si–B alloy reveals substantially larger $R_{ct} = 2596$ Ω cm^2 compared to the other Ni-based amorphous alloys. Generally, the charge transfer resistance R_{ct} for the alloys with Mo is substantially smaller than that of the Ni–(Ta,Nb)–B and Ni–Si–B alloys. The results on the charge transfer resistance, R_{ct}, correlate with those for i_o for all investigated alloys. The double layer capacitance, C_{dl}, determined for the Ni-based amorphous alloys, is similar, revealing that the surface area of the studied glassy ribbons is comparable. This fact is expected due to the same technology (rapid quenching by melt-spinning) used for the ribbons production, followed by identical mechanical polishing. Here, it is necessary to be mentioned that whereas all amorphous ribbons were produced by the same method and their surfaces are generally very smooth, the crystalline Ni plate, although polished in the same way, revealed in fact higher roughness than the glassy ribbons (Fig. 6). Therefore, the data for Ni, having larger real surface area, cannot be consistently compared with those for the amorphous alloys.

Judging from the exchange current values i_o and the hydrogen overpotential at certain i (e.g., 10 mA cm^{-2}, η_{10}), the Ni-based amorphous alloys studied reveal lower electrocatalytic activity for HER compared to pure crystalline Ni. It is, however, known [8] that some amorphous alloys produced by melt-spinning contain thin oxide films, formed generally during the rapid quenching, and when this film is removed by chemical etching they significantly improve their activity. For the Ni-based amorphous alloys, a pretreatment with HF was found to substantially enhance the electrocatalytic activity either by removing the surface
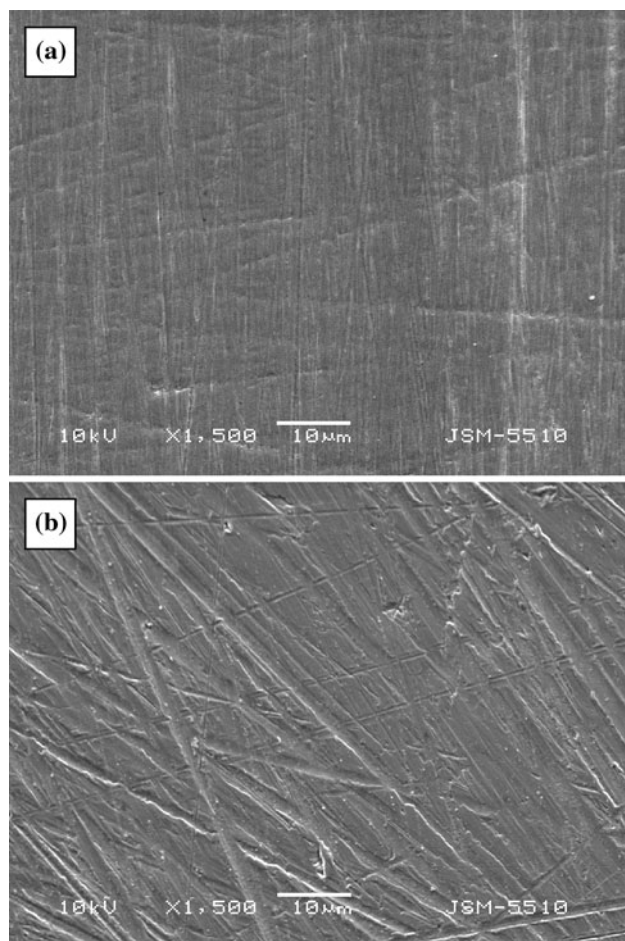
Fig. 6 Typical amorphous ribbon ($Ni_{66.5}Mo_{28.5}B_5$) surface (**a**) and Ni plate surface (**b**) after polishing

oxide layers or by increasing the roughness factor [21]. Chemical pretreatment may, however, also change the surface chemical composition of the alloy as well as its porosity, making in this way the direct comparison between the catalytic activity of the amorphous alloys unreasonable. Therefore, in the present study, we have treated the surface of the amorphous ribbons only mechanically in order to eliminate the surface oxides and thus to be able to compare the catalytic activity of Ni-based amorphous alloys with different composition. The surface composition of the alloys was proved by XPS analysis to correspond to that of the ribbons bulk.

Among the studied amorphous alloys, $Ni_{66.5}Mo_{28.5}B_5$ shows the lowest η_{10}; that of $Ni_{63}Mo_{27}B_{10}$ is a little higher and Ni–Si–B reveals the highest η_{10} value (Table 1). $Ni_{66.5}Mo_{28.5}B_5$ shows also slightly higher i_o than $Ni_{63}Mo_{27}B_{10}$. Comparing the R_{ct} of the alloys, it is seen that Ni–Mo–B alloys have lower charge transfer resistance than the other amorphous materials, as that of $Ni_{66.5}Mo_{28.5}B_5$ is 4.5 times lower than that of $Ni_{63}Mo_{27}B_{10}$. The results from the EIS are in agreement with the polarization measurements.

The pseudo-eutectic Ni–(Ta,Nb)–B amorphous alloys show clear decrease of their catalytic activity in the potential range of $\eta = -100/-200$ mV, followed, however, by rapid increase at $\eta < -200$ mV. The decrease of the catalytic activity of these alloys corresponds to the potentials, where hydrogen absorption into the amorphous alloys has been clearly detected (see the peaks in the polarization curves at about -1.1 V, Fig. 2a). The last was also proved by galvanostatic hydrogen charge/discharge experiments. Figure 7 shows galvanostatic discharge curves at 25 μA cm^{-2} of preliminary charged (100 μA cm^{-2} for 1 h) Ni–Nb–B and Ni–Ta–B alloys. The amount of hydrogen determined from the discharge curve is small, but having in mind the insignificant real surface area of the electrode (amorphous ribbons with smooth surfaces), it can be concluded that the alloys do absorb hydrogen under the electrochemical conditions applied. Obviously, the hydrogen absorption process is associated with an initial decrease of the catalytic activity. The absorbed hydrogen (most probably mainly in the near surface region, judging from the amount of absorbed hydrogen), however, results in a change of the surface electronic structure, which leads to an increase of the catalytic activity of the alloy at $\eta < -200$ mV (b_c decreases). The last can be also connected with the removal of the surface oxides, when the intensity of the HER increases. Similar result was also observed for the Ni–Si–B alloys, but in a much smaller degree.

Since the surface of all investigated Ni-based alloys was mechanically polished in the same way before the electrochemical experiments as well as they are all fully amorphous, it can be concluded that the observed variations in the electrocatalytic behavior for HER have to be related mainly to their different chemical composition. Among the alloys studied, the Ni–Mo–B amorphous alloys
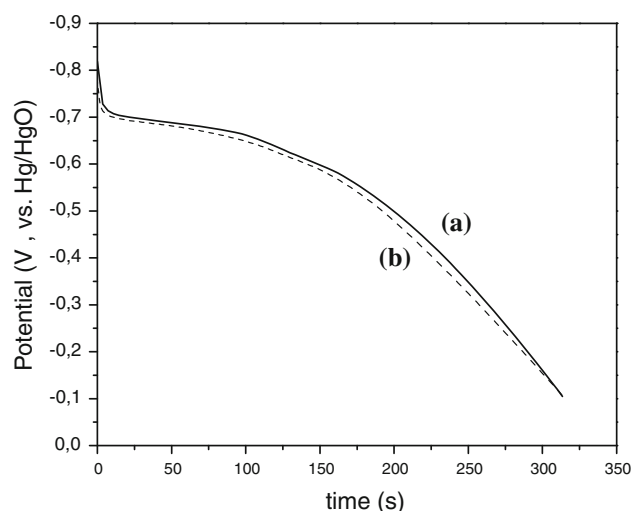

Fig. 7 Galvanostatic hydrogen discharge of $Ni_{78.5}Nb_3B_{18.5}$ (**a**) and $Ni_{78.5}Ta_3B_{18.5}$ (**b**) at 25 μA cm^{-2}

show the best combination of η_{10}, i_o, and R_{ct}, as between them the $Ni_{66.5}Mo_{28.5}B_5$ alloy has slightly higher activity for HER. The amorphous alloys containing Nb and Ta, as well as the Ni–Si–B alloy absorb hydrogen during the polarization experiments at about $\eta = -100$ mV, which was found to have a complex effect (generally positive) on their electrocatalytic behavior. Ni–Mo–B amorphous alloys do not show clear hydrogen absorption during the polarization experiments.

Conclusion

Ni-based amorphous alloys were synthesized by rapid solidification from the melt. The electrocatalytic activity of the as-quenched glasses with respect to the HER in alkaline water electrolysis was studied in relation to the alloy composition. The kinetic parameters of the HER were evaluated by cyclic voltammetry and impedance spectroscopy techniques in 6 M KOH at room temperature. It was obtained that the molybdenum containing amorphous alloys (Ni–Mo–B) showed an increased electrocatalytic activity in the HER compared to the other Ni-based amorphous alloys studied, which can only be attributed to the improved intrinsic activity of the material, because of the identical surface roughness of all amorphous ribbons studied. Noticeable hydrogen absorption was also observed for the Ni-based amorphous alloys containing Nb, Ta, and Si, which was found to have a complex influence on their catalytic activity.

References

1. Shan Zh, Liu Y, Chen Zh, Warrender G, Tian J (2008) Int J Hydrogen Energy 33:28
2. Brunelli K, Dabala M, Frattini R, Sandona G, Calliari I (2001) J Alloys Compd 317–318:595
3. Brookes HC, Carruthers CM, Doyle B (2005) J Appl Electrochem 35:903
4. Brunelli K, Dabala M, Frattini R, Magrini M (2003) J Appl Electrochem 33:995
5. Gebert A, Mattern N, Kuhn U, Eckert J, Schultz L (2007) Intermetallics 15:1183
6. Metikos-Hukovic M, Jukic A (2000) Electrochim Acta 45:4159
7. Kirk DW, Thorpe SJ, Suzuki H (1997) Int J Hydrogen Energy 22(5):493
8. Jukic A, Piljac J, Metikos-Hukovic M (2001) J Mol Catal A 166:293
9. Losiewicz B, Stepien A, Gierlotka D, Budniok A (1999) Thin Solid Films 349:43
10. Panek J, Serek A, Budniok A, Rowinski E, Lagiewka E (2003) Int J Hydrogen Energy 28:169
11. Losiewicz B, Budniok A, Rowinski E, Lagiewka E, Lasia A (2004) J Appl Electrochem 34:507
12. Kubisztal J, Budniok A, Lasia A (2007) Int J Hydrogen Energy 32:1211
13. Panek J, Budniok A, Łągiewka E (2007) Rev Adv Mater Sci 15:234
14. Popczyk M (2007) Phys Chem Solid State 8(4):767
15. Rami A, Lasia A (1992) J Appl Electrochem 22:376
16. Chen L, Lasia A (1992) J Electrochem Soc 139:3458
17. Tanaka S, Hirose N, Tanaki T (1999) J Electrochem Soc 146:2477
18. Chen L, Lasia A (1992) J Electrochem Soc 139:3214
19. Jaksic JM, Vojnovic MV, Krstajic NV (2000) Electrochim Acta 45:4151
20. Rosalbino F, Borzone G, Angelini E, Raggio R (2003) Electrochim Acta 48:3939
21. Spirano S, Baricco M, Antonione C, Angelini E, Rosalbino F, Spinelli P (1994) Electrochim Acta 39:1781